JOURNAL OF MATERIALS SCIENCE 13 (1978) 523–533

A study on titanium diffusion into $LiNbO_3$ waveguides by electron probe analysis and X-ray diffraction methods

KIYOMASA SUGII, MASAHARU FUKUMA, HIROSHI IWASAKI
Musashino Electrical Communication Laboratory, Nippon Telegraph and Telephone Public Corporation, Musashino-shi, Tokyo, 180, Japan

The diffusion of titanium into lithium niobate has been studied by X-ray rocking curve and topographic methods as well as electron probe microanalysis in an attempt to determine the diffusion mechanism and evaluate the crystallinity of the diffused layer. It was found that the titanium concentration along the depth in the diffused layer approximates to a Gaussian distribution, the activation energy for diffusion being 2.18 eV. We also found that the diffusion of titanium caused a marked lattice contraction along the *a*-axis ($\Delta a/a \approx -10^{-3}$) resulting in the generation of misfit dislocations and cracks in the diffused layer. The high activation energy and the lattice contraction suggest that the titanium ions diffuse substitutionally into the lithium niobate crystal. Mechanisms causing refractive index changes in the diffused layer are also discussed.

1. Introduction

Diffusion of Ti into $LiNbO_3$ has been used in the making of optical waveguides since it causes very large increments in the refractive indices n_0 and n_e [1, 2]. However, few studies have been made on diffusion mechanisms of Ti, crystallinity of the diffused layer, and mechanisms causing the refractive index changes. The fact that Ti ions sit on well defined sites in $LiNbO_3$ has recently been made clear by X-ray photoelectron spectroscopy [3]. Using the X-ray rocking curve method, we found a marked contraction of lattice constant a, which was closely related to the generation of defects and the refractive index changes in the diffused layer.

This paper investigates the diffusion mechanism and the defect structures occurring in the diffused layer and proposes mechanisms for the refractive index changes.

2. Experimental

2.1. Preparation of samples

The samples were prepared using a technique very similar to that commonly used to produce optical waveguides, however with a hot-pressed TiO_2 ceramic plate used as a sputtering target. A thin film of TiO_2 of thickness τ was first sputtered onto a polished surface of a Y-plate $LiNbO_3$ crystal and then the crystal was heated at temperature T in air for time t. Two groups of samples were made as follows: Group I consisted of three samples diffused under the conditions $\tau = 500$ Å, $T = 1000$, 1050, and 1100° C, and $t = 10$ h; Group II consisted of four samples diffused under the conditions $\tau = 300$ Å, $T = 1000$° C, and $t = 1.25$, 2.5, 3.75, and 10 h. The samples of group I were made to examine relationships between impurity concentrations, strains, and refractive index changes in the diffused layers, and those of group II to investigate generation mechanisms for diffusion-induced defects.

2.2. Measurement of Ti distribution in the diffused layer

Electron probe microanalysis (EPMA) was employed to measure Ti distribution against depth in a sample which had been sliced to obtain a cross-section of the diffused layer. Measuring conditions of the EPMA were as follows: a scanning speed for the sample of 1 μm min^{-1}, and

an electron beam diameter of about 1 μm with an accelerating voltage of 15 kV and an absorbing current of 6×10^{-9} A. The Ti atomic fraction in the diffused layer could be determined by using the response R_0 from a TiO_2 ceramic standard of about 2000 cps. The ceramic was assumed to have an atomic concentration of Ti, $N(\mathrm{Ti}) = 3.28 \times 10^{22}$ cm^{-3}. The measurements of Ti distribution were made only for group I samples, since their diffusion depth was large enough to be accurately determined by EPMA.

2.3. Measurement of strains in the diffused layer

The X-ray rocking curve method was employed for precise determination of strains in the diffused layer. Rocking curves were taken using a triple-crystal spectrometer [4] as shown in Fig. 1. It consists of two nearly perfect germanium single crystals C_1 and C_2, and a sample crystal C_3 arranged in the (+, +, −) position. For C_1 and C_2 the symmetric (3 3 3) reflection was used, the Bragg angle for Cu$K\alpha_1$ radiation, θ, being about 45°. The angular and wavelength distributions of the X-ray beam diffracted from the second crystal C_2 were $\omega = 2 \times 10^{-5}$ rad (4″ arc) and $\Delta\lambda/\lambda_0 = 2 \times 10^{-5}$ ($\lambda_0 = 1.5405$ Å), respectively. They were small enough to obtain an intrinsic rocking curve of the sample for any lattice plane ($h\,k\,l$). In addition, the beam thus obtained is almost σ-polarized (an electric field vector E perpendicular to the plane of incidence) because the scattering angle, 2θ, is near 90°. A slit was placed between C_2 and C_3 to obtain a beam of width 0.5 mm and height 2.0 mm. Undiffused samples produced (0 3 0) rocking curves with width at half maximum intensity (WHMI) of about 12″ arc, which is essentially the theoretical

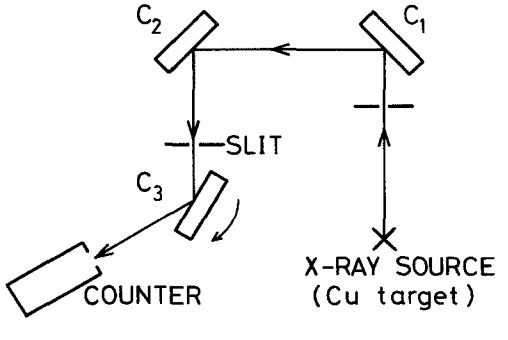

Figure 1 Schematic arrangement of a triple-crystal spectrometer.

WHMI for the (0 3 0) reflection of a perfect $LiNbO_3$ crystal under these experimental conditions. On the other hand, the diffused samples produced (0 3 0) rocking curves accompanied by a diffraction satellite, displaced in angle with respect to the diffraction peak of the unperturbed region in the substrate. Precise determination of strains in the diffused layer is possible since a standard of lattice constant is available in the same trace as the diffused layer. The strain along the a-axis, ϵ_y (ϵ_x), is obtained from a shift in angle $\theta_{0\,3\,0}$ of the satellite as:

$$\epsilon_y = \frac{\Delta a}{a} = -\frac{\Delta\theta_{0\,3\,0}}{\tan\theta_{0\,3\,0}} \tag{1}$$

where $\theta_{0\,3\,0}$ is the Bragg angle for the (0 3 0) reflection. However, strain along the c-axis, ϵ_z, cannot be directly measured on the diffused layer, since the c-axis is parallel to the surface in the Y-plate crystal. If a shift $\Delta\theta_{h\,k\,l}$ can be obtained for a ($h\,k\,l$) reflection with non-zero l, the strain ϵ_z is calculated from a pair of shifts $\Delta\theta_{0\,3\,0}$ and $\Delta\theta_{h\,k\,l}$ using the following expression:

$$\epsilon_z = \frac{\Delta C}{C} = \left(\frac{C^2}{l^2}\right)\left[\frac{1}{d}\left(-\frac{\Delta\theta_{h\,k\,l}}{\tan\theta_{h\,k\,l}}\right) - \frac{4}{3}\left(\frac{h^2 + hk + k^2}{a^2}\right)\left(-\frac{\Delta\theta_{0\,3\,0}}{\tan\theta_{0\,3\,0}}\right)\right] \tag{2}$$

where d is the ($h\,k\,l$) lattice spacing and $\theta_{h\,k\,l}$ is the Bragg angle for the ($h\,k\,l$) reflection. A (0 3 6) reflection was used for this purpose. The geometrical relationship between the (0 3 6) lattice plane and the surface is shown in Fig. 2. The angle β is an interplanar angle between the (0 3 6) plane and the surface. In the (0 3 6) asymmetric reflection, a shift $\Delta\theta^{+}_{0\,3\,6}$ for an incident beam with a glancing angle ($\theta_{0\,3\,6} + \beta$) is generally not equal to a shift $\Delta\theta^{-}_{0\,3\,6}$ for one with a glancing angle ($\theta_{0\,3\,6} - \beta$), since an inclination of the (0 3 6) lattice plane, $\Delta\beta$, is involved in both shifts (see Fig. 2b). It is readily shown that $(\Delta\theta^{+}_{0\,3\,6} + \Delta\theta^{-}_{0\,3\,6})/2$ gives $\Delta\theta_{0\,3\,6}$ to be substituted in Equation 2, which is a shift due only to the difference in the (0 3 6) lattice spacing between the diffused layer and the substrate.

2.4. Observation of diffusion-induced defects

The diffused layer and substrate can be diffracted separately by utilizing the diffraction angle cor-

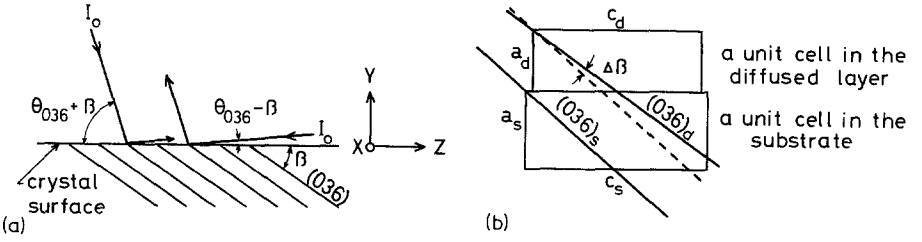

Figure 2 (a) Relationship between the (0 3 6) lattice plane and the incident X-ray beam. (b) Inclination in the (0 3 6) lattice planes between the substrate and the Ti-diffused layer. The dotted line represents a lattice plane parallel to $(0\ 3\ 6)_s$.

responding to each lattice constant. Thus separate topographs can be recorded for the diffused layer and substrate. This technique is very useful for the investigation of defects generated by diffusion. We took topographs of the Ti-diffused layer using the Lang camera applied to the reflection case with Cu$K\alpha_1$ radiation.

3. Results

3.1. Ti distributions in the diffused layers

Fig. 3 shows the Ti distributions of the samples of group I. Here, a position on the chart was regarded as the surface at which an EPMA response decayed to a value halfway between the maximum and background levels. All the diffused layers have bell-shaped Ti distributions characteristic of the Gaussian distribution. The Gaussian distribution $C(y)$ is expressed as follows:

$$C(y) = C_s \exp(-y^2/b^2), \tag{3}$$

$$C_s = \rho\tau/2(\pi Dt)^{-1/2}, \tag{4}$$

$$b^2 = 4Dt \tag{5}$$

where y is the depth below the surface, ρ is the number of atoms per unit volume in the deposited film of thickness τ, and D is the diffusion coefficient given by

$$D = D_0 \exp(-Q_d/kT). \tag{6}$$

Values of the EPMA response at the surface, R_s, corresponding to C_s, and of the diffusion coefficient D could be determined in such a way that

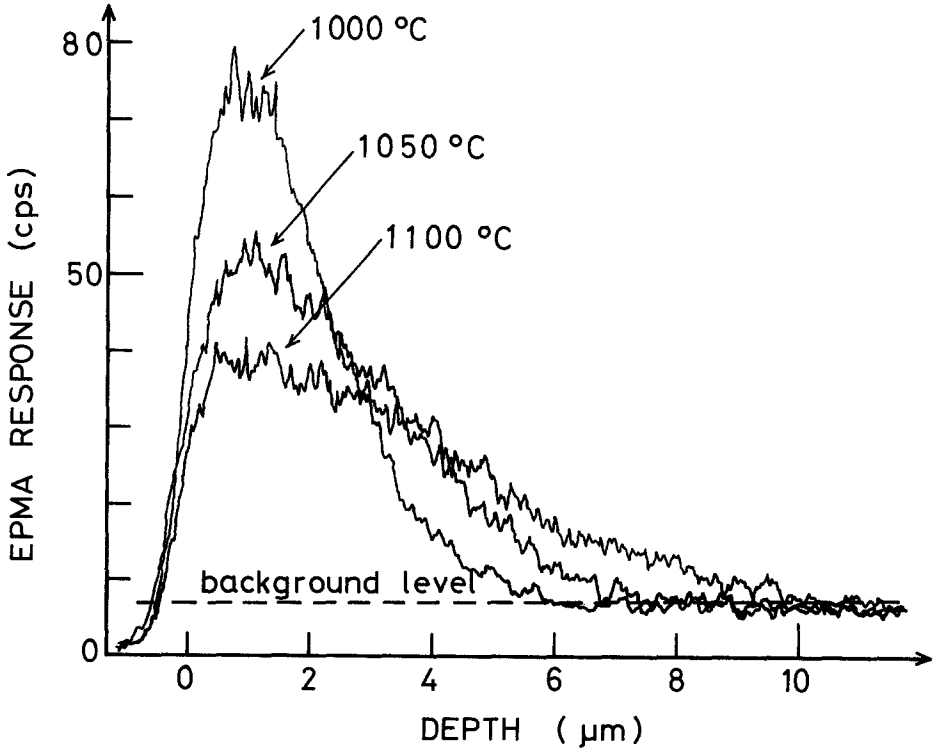

Figure 3 Ti distribution as determined by EPMA of slices for the samples of group I.

TABLE I Titanium atomic fractions at crystal surface, N_s(Ti), and diffusion coefficients, D, for the samples of group I. (Diffusion time $t = 10$ h)

T(° C)	N_s(Ti)(10^{21} cm^{-3})	D(10^{-12} cm^2 sec^{-1})
1000	1.23	0.506
1050	0.82	1.06
1100	0.57	2.13

the theoretical distribution calculated by Equations 3 to 5 was fitted to the measured one. Then, the Ti atomic fraction at the surface N_s(Ti) was estimated from a ratio of R_s to R_0 on the assumption that the EPMA response was proportional to $C(y)$. The calculated values of N_s(Ti) and D are given in Table I. It is to be noted that Ti has a remarkably high solubility in $LiNbO_3$ in the temperature range 1000 to 1100° C. The diffusion coefficients D are plotted against $1/T$ in Fig. 4. The straight line was calculated by the least squares method. The diffusion data were calculated as $D_0 = 2.19 \times 10^{-4}$ cm^2 sec^{-1} and $Q_d = 2.18$ eV.

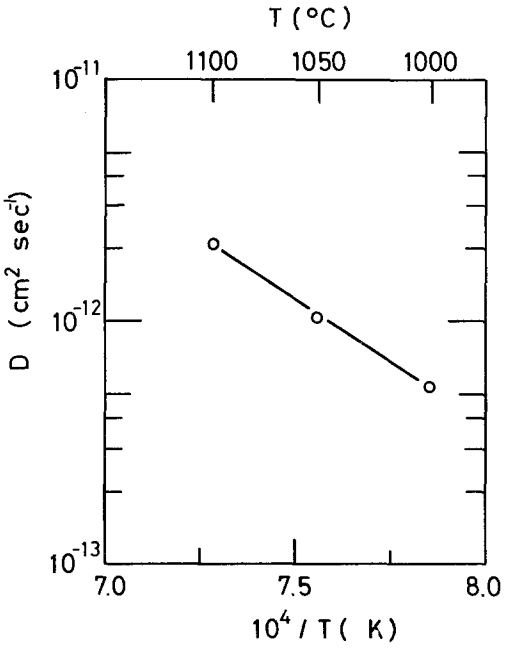

Figure 4 Variation of diffusion coefficient, D, with temperature as $1/T$ for the samples of group I.

3.2. Strains in the diffused layers

Fig. 5 shows (0 3 0) rocking curves for the samples of group I and group II, respectively. The satellite peak corresponds to the lattice constant of the diffused layer nearest the surface, since only the surface has a Ti concentration sufficiently uniform for a well defined diffraction peak to be formed. Contraction of the lattice constant a was observed in the diffused layers of all the samples investigated in this study. Fig. 6 shows three pairs of (0 3 6) rocking curves $\Delta\theta^+_{036}$ and $\Delta\theta^-_{036}$ of the samples of group II, which correspond to those shown in Fig. 5b. The ratio of satellite to substrate peak intensity increases with diffusion time t, although the absolute intensity becomes small, due to the effect of asymmetric reflection [5]. For the samples of group I, the substrate peaks could hardly be detected since they were absorbed by the thick diffused layers.

Using Equations 1 and 2, we could calculate the strains ϵ_y and ϵ_z. The strains ϵ_y for the samples of group I are given in Table II. A linear relationship is found between $\ln(\epsilon_y)$ and $1/T$ as shown in Fig. 7. The strains ϵ_y and ϵ_z for the samples of group II are given in Table II. The strain ϵ_z is about one order of magnitude smaller than the strain ϵ_y in each sample, and so the strain ϵ_z is neglected in this paper. The strains ϵ_y are plotted against t in Fig. 8. The slope of $\ln(\epsilon_y)$ versus $\ln(t)$ plot is calculated as $-\frac{1}{2}$.

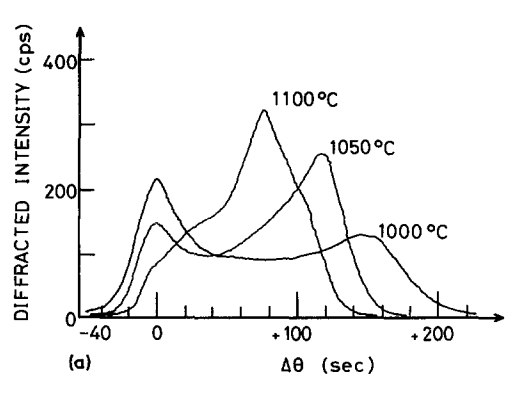

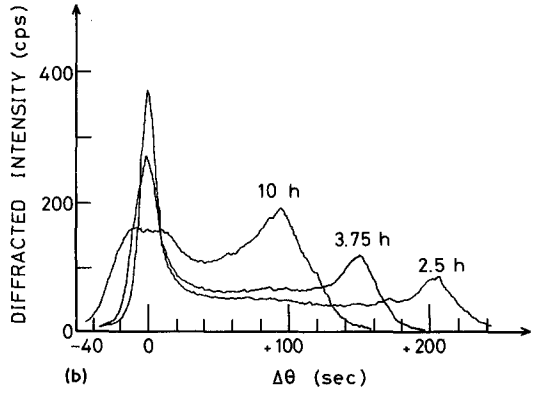

Figure 5 Families of (0 3 0) rocking curves for the samples of (a) group I and of (b) group II.

TABLE II Strains in the Ti-diffused layer of $LiNbO_3$.

Samples of group I (t = 10 h)		Samples of group II (T = 1000° C)		
T (° C)	$\epsilon_y \times 10^3$	t (h)	$\epsilon_y \times 10^3$	$\epsilon_z \times 10^4$
1000	−1.3	1.25	−2.19	1.2
1050	−0.71	2.50	−1.66	0.75
1100	−0.39	3.75	−1.28	0.62
–	–	10	−0.759	0.52

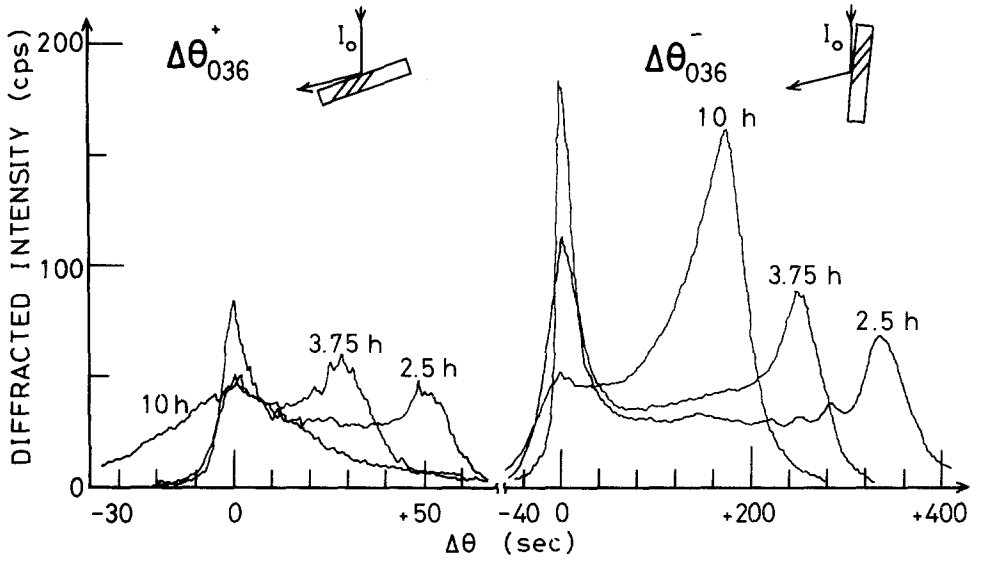

Figure 6 Family of (0 3 6) rocking curves for the samples of group II.

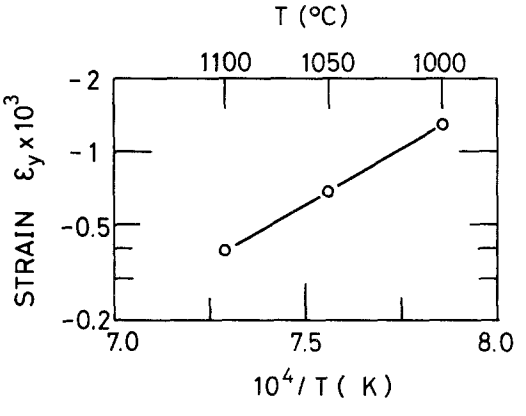

Figure 7 Variation of strain ϵ_y with temperature as 1/T for the samples of group I.

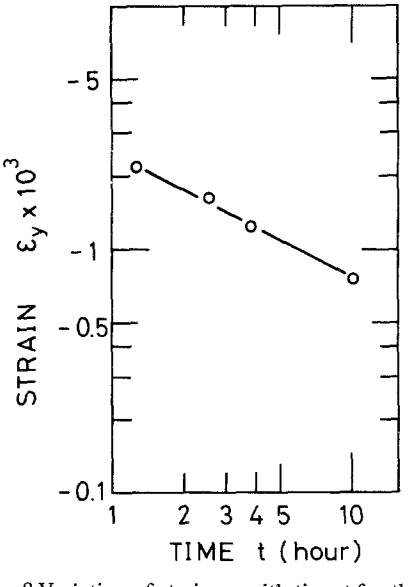

Figure 8 Variation of strain ϵ_y with time t for the samples of group II.

These two relationships found between ϵ_y and $1/T$, and between ϵ_y and t are similar to those between C_s and $1/T$, and between C_s and t, respectively. Therefore, we can conclude that the strain ϵ_y in the diffused layer is proportional to the surface concentration C_s.

3.3. Defects in the diffused layers

Fig. 9 shows topographs of the diffused layers of the samples of group I. The excess diffraction contrast observed in all the samples is due to a high density of defects. It is found that the higher the diffusion temperature, the less serious the degradation in crystallinity in the diffused layer. This corresponds to the result obtained by the

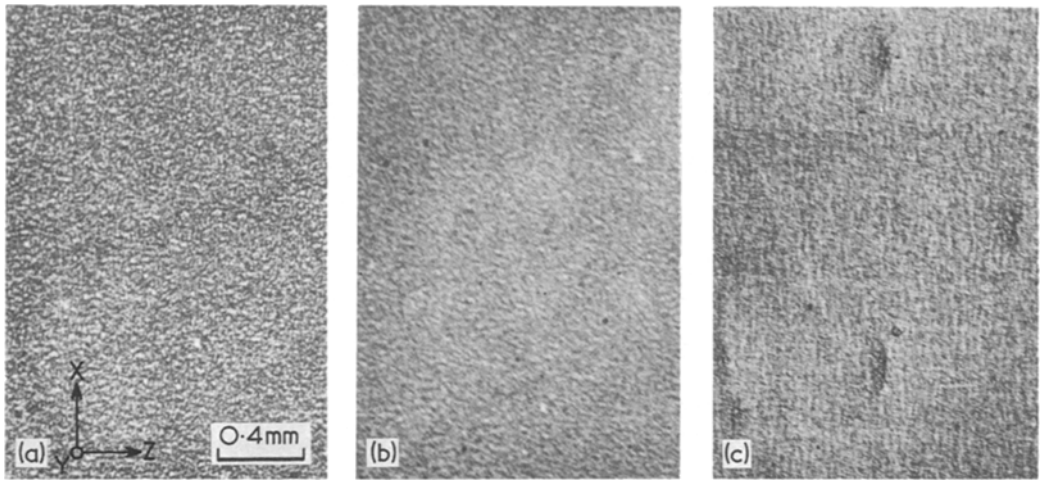

Figure 9 Diffusion-induced defects in the Ti-diffused layers of the samples of group I ($g = 0\,3\,0$). (a) 1000° C, 10 h, (b) 1050° C, 10 h, (c) 1100° C, 10 h.

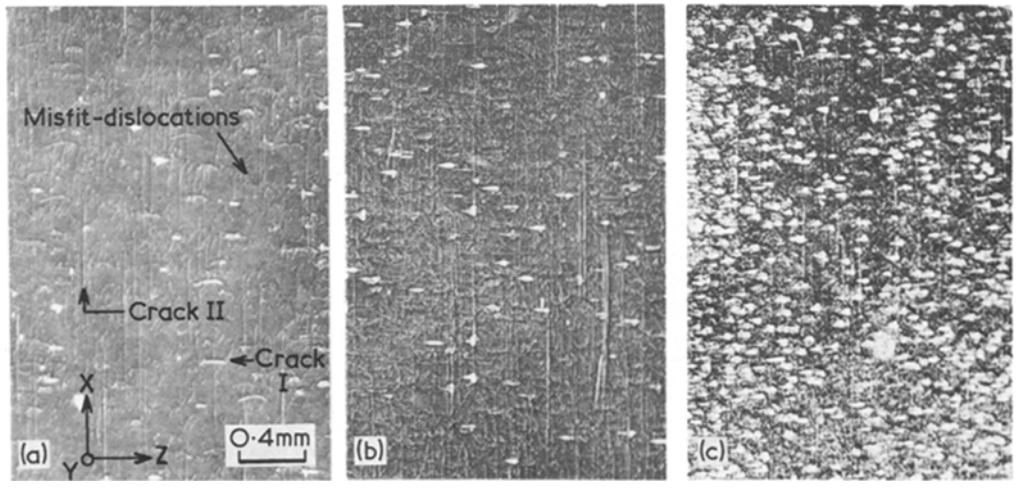

Figure 10 Diffusion-induced deffects in the Ti-diffused layers of the samples of group II ($g = 0\,3\,0$). (a) 1000° C, 2.5 h, (b) 1000° C, 3.75 h, (c) 1000° C, 10 h.

rocking curve measurement that the strain decreased with increasing diffusion temperature from 1000 to 1100° C.

Fig. 10 shows topographs of the diffused layers of some samples of group II. Three types of defects are clearly observed: misfit-dislocations, cracks of type I running in the direction perpendicular to the X-axis, and cracks of type II running in the direction perpendicular to the Z-axis. All of the defects were induced by the Ti diffusion. Misfit-dislocations should be generated so as to relieve stresses in the diffused layer. The directions of the cracks suggest that the type I cracks must be generated by a stress along the a-axis and the type II cracks by a stress along the c-axis. Densities of the misfit-dislocations and of the type I cracks increase with diffusion time t, however, the density of type II cracks is almost independent of t.

When the Ti-diffused layer is utilized as an optical waveguide, the defects may increase the scattering loss of optical guided waves as observed in the Nb-diffused $LiTaO_3$ waveguides [6].

4. Discussion

4.1. Diffusion sites for Ti ions in $LiNbO_3$

Lattice contraction due to the presence of substitutional ions has been observed in the case of diffusion of such atoms as B and P into Si [7]. These substitutional atoms also have activation

energies of about 3.7 eV which are much higher than those for interstitial atoms, such as Li and Cu, of about 1 eV [8]. Therefore, both the marked lattice contraction and the high activation energy found in the Ti diffusion into $LiNbO_3$ imply that Ti diffuses substitutionally into $LiNbO_3$ crystal. Recently it has been shown that Ti diffused into $LiNbO_3$ is all +4 valent and Ti ions sit not on vacancies or defects but on well defined sites [3]. In $LiNbO_3$, two possible sites remain for substitutional impurities; a Li site and a Nb site. The lattice contraction would occur if Ti ions replaced either the Li site or the Nb site, since the effective ionic radius of Ti^{+4}, 0.605 Å, is smaller than those of Li^{+1} and Nb^{+5} of 0.68 and 0.64 Å, respectively, when the coordination number of all of them is 6 [9]. However, the replacement of Nb ions by Ti ions is more favourable from the point of view of charge compensation, so it is assumed that Ti is diffused as substitutional ions for the Nb site in $LiNbO_3$.

4.2. Theoretical rocking curve from a diffused crystal

A rocking curve profile can be calculated for a diffused crystal on the assumption that strain ϵ_y is proportional to Ti concentration. A diffused layer in which the strain changes gradually is approximated to by an N-step multilayer structure as shown in Fig. 11. The layer thickness, y_i, was determined in such a way that each layer had an equal variation of strain within it. Then, the ith layer was considered to diffract an incident beam I_0 as a perfect crystal with thickness y_i and lattice constant $a(1 + \epsilon_i)$, where ϵ_i is the mean strain in the ith layer. A number of steps, N, was chosen so that the separation in diffraction angle between adjacent layers, $(\epsilon_i - \epsilon_{i-1}) \tan\theta$, was 10 sec of arc, which was an appropriate value for obtaining an integrated diffraction intensity of the ith layer without any interference due to other layers for the incident beam used in this study. From the dynamical theory of X-ray diffraction [10], the integrated diffraction intensity from a thin film is expected to increase with film thickness until the thickness reaches a value of ξ, which is the penetration depth of X-ray fields over the angular range for which "total reflection" is occurring. The penetration depth for a $(h\,k\,l)$ reflection in the symmetric Bragg case is given by [11].

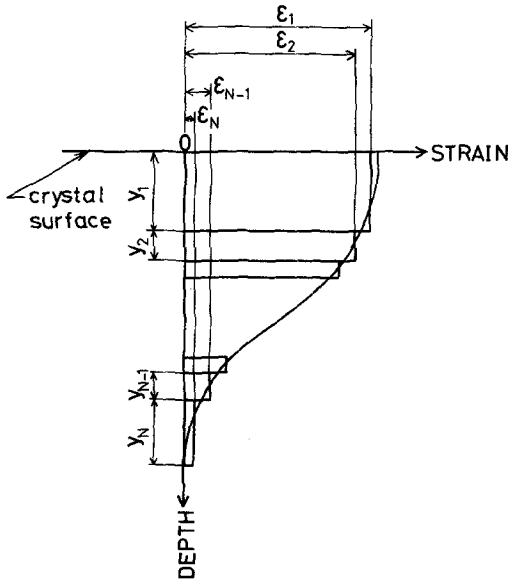

Figure 11 Approximation of a staircase function. The Ti-diffused region in which a strain changes gradually is approximated by an N-step multilayer structure.

$$\xi = V/(2|P|r_e\lambda_0 F_{h\,k\,l}) \tag{7}$$

where V is the unit cell volume, P is the polarization factor which equals unity or $\cos 2\theta$ for the σ-polarization state and π-state **E** in the plane of incidence, respectively. r_e is the classical electron radius, and $F_{h\,k\,l}$ is the structure factor. Using this expression, ξ for the σ-polarization state is calculated as 4.2 μm for the (0 3 0) reflection of $LiNbO_3$ at $\lambda_0 = 1.5405$ Å. Thus, fractions of the incident beam to be diffracted by the ith layer and by the substrate with thickness larger than ξ are given by

$$I_i/I_0 = R(y_i/\xi) \exp\left[-2\mu_0\left(\sum_{k=0}^{i-1} y_k\right)/\sin\theta_{0\,3\,0}\right], \tag{8}$$

and

$$I_s/I_0 = R\exp\left[-2\mu_0\left(\sum_{k=0}^{N} y_k\right)/\sin\theta_{0\,3\,0}\right] \tag{9}$$

respectively, where R is the reflection coefficient, μ_0 is the normal absorption coefficient of $LiNbO_3$ for Cu$K\alpha_1$ of about 470 cm^{-1}, and $y_0 = 0$.

In order to show the sensitivity of a type of impurity distribution on a rocking curve profile, we calculate the (0 3 0) rocking curve profiles for two typical cases: (a) exponential distribution; $C(y) = C_s \exp[-y/2\sqrt{(Dt)}]$, and (b) Gaussian; $C(y) = C_s \exp(-y^2/4Dt)$, provided that they

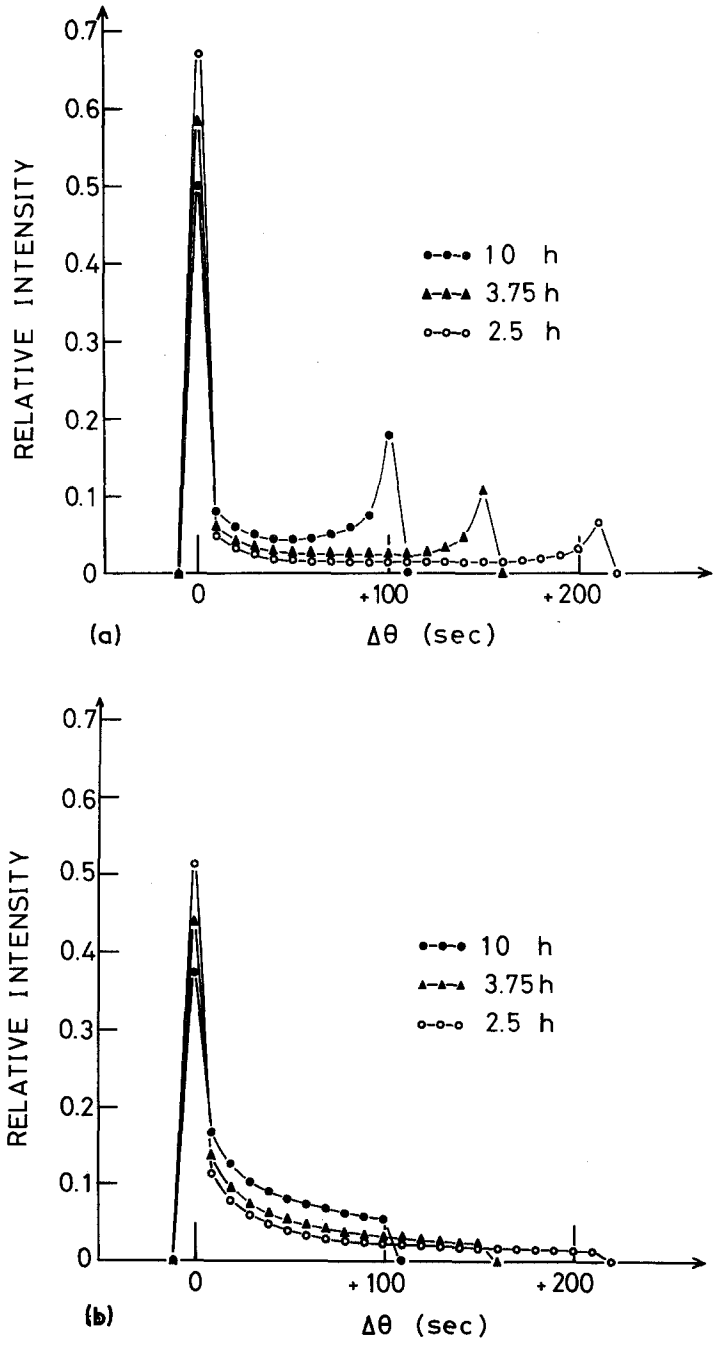

Figure 12 Theoretical (0 3 0) rocking curves for the samples of group II (see Fig. 5b). (a) Gaussian strain field, (b) exponential one.

produced strain distributions as $\epsilon(y) = \epsilon_s \exp [-y/2\sqrt{(Dt)}]$ and $\epsilon(y) = \epsilon_s \exp(-y^2/4Dt)$; respectively. Here, ϵ_s was taken as ϵ_y, as given in Table II. Fig. 12 shows (0 3 0) rocking curves calculated for the samples of group II. The experimental profiles (Fig. 5b) were more similar to those calculated for the Gaussian distribution than to the exponential case, especially for samples with diffusion times of 2.5 and 3.75 h. However, for the sample of diffusion time of 10 h, the experimental profile differs from that calculated even for the Gaussian distribution. It is considered that the strain field was transformed from the initial Gaussian distribution, probably due to generation of a high-density of defects near the surface. The observed ratio of the satellite intensity to substrate is about twice as large as the calculated ratio. This is reasonable since, for very thin layers, the integrated diffraction intensity becomes larger than that

predicted by the dynamical theory of X-ray diffraction.

4.3. Mechanism for generation of misfit-dislocations and cracks

The diffusion of Ti into $LiNbO_3$ created stresses sufficient to generate both misfit-dislocations and cracks within the diffused layer. In evaluating stresses, we use a positive sign for tensile stress and a negative one for compressive stress. By assuming that the stress σ_y on the diffused layer in the direction normal to the surface plane is zero, the maximum impurity-induced stresses along the crystal surface inside the diffused layer can be expressed as follows:

$$(\sigma_x)_{\max} = \frac{1}{(s_{11}s_{33} - s_{13}^2)} \{-s_{33}\epsilon_y + s_{13}\epsilon_z\}$$

$$\approx -\frac{s_{33}\epsilon_y}{(s_{11}s_{33} - s_{13}^2)} \quad (10)$$

$$(\sigma_z)_{\max} = \frac{1}{(s_{11}s_{33} - s_{13}^2)} \{s_{13}\epsilon_y - s_{11}\epsilon_z\}$$

$$\approx \frac{s_{13}\epsilon_y}{(s_{11}s_{33} - s_{13}^2)} \quad (11)$$

where s is the compliance of $LiNbO_3$ [12]. The calculated stresses for the samples of groups I and II are given in Table III. These stresses were partially relieved by the generation of misfit-dislocations near the interface between the diffused and substrate regions, however the presence of cracks indicate that the density of the misfit-dislocations was much lower than a density needed for complete accommodation of the impurity-induced stresses. Anisotropy of stresses, $(\sigma_x)_{\max} > (\sigma_z)_{\max}$, resulted in preferential generation of type I cracks.

TABLE III Calculated stresses in the Ti-diffused layer of $LiNbO_3$.

t (h)	$(\sigma_x)_{\max}$ (kg cm^{-2})	$(\sigma_z)_{\max}$ (kg cm^{-2})
2.50	3.0×10^3	9.1×10^2
3.75	2.3×10^3	7.0×10^2
10	1.2×10^3	3.6×10^2

4.4. Mechanisms causing refractive index changes in the diffused layer

There are at least three possible mechanisms for refractive index changes in the diffused layer, as follows: (i) due to a photoelastic effect by diffusion-induced strains. (ii) due to increasing of the electronic polarizability by the in-diffusion of Ti. (iii) due to decreasing of the spontaneous polarization of $LiNbO_3$, P_s, by Ti diffusion.

The refractive index of a crystal is specified by the indicatrix, that is, an ellipsoid whose coefficients are the components of the relative dielectric impermeability tensor B_{ij}, namely,

$$B_{ij}x_ix_j = 1. \quad (12)$$

Strains S_n deform the indicatrix through the photoelastic effect, and the change in B_{ij} is given by

$$\Delta B_{ij} = p_{ij.n}S_n. \quad (13)$$

In the case of a thin layer of diffusion, it is sufficient to consider only principal strains S_1, S_2, and S_3, in the X-, Y-, and Z-axes, respectively. Then, Equation 13 turns into

$$\Delta B_1 = \Delta B_2 = -(p_{11}S_1 + p_{12}S_2 + p_{13}S_3), \quad (14)$$

$$\Delta B_3 = -(p_{31}S_1 + p_{31}S_2 + p_{33}S_3), \quad (15)$$

where all the suffixes are abbreviated in the matrix form [13]. By taking $|\epsilon_x| = |\epsilon_y| \gg \epsilon_z$ into consideration, changes in the refractive indices at the surface are approximated by

$$\Delta n_0 \approx -\frac{n_0^3}{2}(p_{11} + p_{12})\epsilon_y, \quad (16)$$

$$\Delta n_e \approx -n_e^3 p_{31}\epsilon_y. \quad (17)$$

For $n_0 = 2.306$, $n_e = 2.220$ (refractive indices for Na D-lines) [14], and $p_{11} = 0.034$, $p_{12} = 0.072$ and $p_{13} = 0.178$ [15], the calculated values for the samples of group I are given in Table IV. By comparing them with the values observed by Noda *et al.* [2], it is found that the refractive index changes due to the photoelastic effect contribute to about half of the observed index changes.

The second possible mechanism for index changes is by diffusion of impurity ions having larger electronic polarizability than that of the

TABLE IV Contribution of the photoelastic effect to the refractive index changes in the Ti-diffused layer of $LiNbO_3$.

	Calculated		Observed*	
T(° C)	$\Delta n_0 \times 10^3$	$\Delta n_e \times 10^3$	$\Delta n_0 \times 10^3$	$\Delta n_e \times 10^3$
1000	0.84	2.5	2.1	3.0
1050	0.46	1.4	1.9	2.5
1100	0.25	0.76	1.8	1.9

*J.NODA, N.UCHIDA, S. SAITO, T. SAKU, and M. MINAKATA, *Appl. Phys. Lett.* 27 (1975) 19.

host ions to be substituted. As in most solids, the refractive index of a ferroelectric crystal should originate from electronic polarization. The relation between the refractive index, n, and electronic polarizability, α, is given as

$$\frac{n^2-1}{n^2+2} = \frac{4\pi}{3}\sum_i N_i\alpha_i(\text{electronic}) \quad (18)$$

where N_i is the number of ions of type i per unit volume and α_i is the electronic polarizability of the ion i. It was found that Ti ions replaced Nb ions of atomic fraction of about 10^{21} cm^{-3} in $LiNbO_3$ crystal. In order to produce a refractive index change $\Delta n = 10^{-3}$, the electronic polarizability of Ti ion, α(Ti), should be larger by 0.04×10^{-24} cm^3 than that of the Nb ion, α(Nb). However, it is unreasonable since the electronic polarizability of ions has a tendency to decrease as ionic radius becomes small [16].

The possibility of a third mechanism is now discussed. In the ferroelectric phase of $LiNbO_3$, one of the characteristic features is the marked decrease in the refractive index due to the spontaneous polarization P_s through the Kerr effect. They are given by

$$\delta n_0 = \tfrac{1}{2} n_0^3 g_{13} P_s^2 \quad (19)$$

$$\delta n_e = \tfrac{1}{2} n_e^3 g_{33} P_s^2 \quad (20)$$

for the refractive indices n_0 and n_e, respectively, where g is the quadratic electro-optic coefficient. If Ti-diffusion into $LiNbO_3$ changed the spontaneous polarization by ΔP_s, ΔP_s would produce refractive index changes given as

$$\Delta n_0 = -n_0^3 g_{13} P_s \Delta P_s, \quad (21)$$

and

$$\Delta n_e = -n_e^3 g_{33} P_s \Delta P_s. \quad (22)$$

When $g_{13} = 0.043\,\text{m}^4\,\text{C}^{-2}$, $g_{33} = 0.16\,\text{m}^4\,\text{C}^{-2}$ [17], and $P_s = 0.50\,\text{C m}^{-2}$ [18], ΔP_s of -0.005 C m^{-2} will cause refractive index changes of $\Delta n_0 \approx 1.3 \times 10^{-3}$ and $\Delta n_e \approx 4.2 \times 10^{-3}$. On the other hand, change of the spontaneous polarization will at the same time cause lattice strains in the a- and c-axes through the electrostrictive effect. Then, strains due to ΔP_s, S_n, are given by

$$S_1 = S_2 = 2Q_{31} P_s \Delta P_s, \quad (23)$$

and

$$S_3 = 2Q_{33} P_s \Delta P_s, \quad (24)$$

where Q is the electrostrictive coefficient: $Q_{31} = -0.0036\,\text{m}^4\,\text{C}^{-2}$ and $Q_{33} = 0.067\,\text{m}^4\,\text{C}^{-2}$ for $LiNbO_3$ [17]. If $\Delta P_s < 0$ as required to increase the refractive indices, it should produce strains $S_2 > 0$, and $S_3 < 0$. The signs of S_2 and S_3, however, are opposite to those of the observed strains ϵ_y and ϵ_z, respectively (see Table II), thus it is unlikely that the refractive index increments are caused by decreasing the spontaneous polarization.

It is concluded that the first mechanism proposed for refractive index changes is more likely than the second and third.

5. Conclusions

A study has been made of the diffusion of titanium into lithium niobate crystal as a function of diffusion time and temperature by the EPMA and X-ray diffraction methods. The results obtained are as follows:

(1) The titanium concentration profile along the depth in the diffused layer approximates to a Gaussian distribution.

(2) The titanium ion has a high activation energy for diffusion, and it also has high solubility in lithium niobate in the temperature range from 1000 to 1100° C.

(3) The titanium diffusion causes marked lattice contraction along the a-axis, which results in generation of misfit-dislocations and cracks in the diffused layer.

(4) Conclusions (2) and (3) suggest that the titanium ion should diffuse substitutionally in the lithium niobate crystal.

(5) The observed X-ray rocking curve profile can be well interpreted by assuming that the amount of lattice contraction is proportional to the titanium concentration.

(6) The most likely mechanism for the refractive index changes in the diffused layer is that due to the photoelastic effect caused by the lattice contraction.

Acknowledgements

The authors would like to thank Dr J. Noda and Dr S. Miyazawa for their helpful discussions and criticisms. Acknowledgement also is due to Mr T. Ikeno of JEOL Ltd. for help with the EPMA measurements.

References

1. R. V. SCHMIDT and I. P. KAMINOW, *Appl. Phys. Lett.* **25** (1974) 458.
2. J. NODA, N. UCHIDA, S. SAITO, T. SAKU, and M. MINAKATA, *ibid* **27** (1975) 19.
3. T. P. PEARSALL, S. CHIANG, and R. V. SCHMIDT, Topical Meeting on Integ. Opt. Salt Lake City, Utah, January 12 (1976) Tech. Digest TuC2-1.
4. M. RENNINGER, *Acta Cryst.* 8 (1955) 1957.
5. P. B. HIRSCH and G. N. RAMACHANDRAN, *ibid* 3 (1950) 187.
6. V. RAMASWAMY and R. D. STANDLEY, *Appl. Phys. Lett.* **26** (1975) 10.
7. B. G. COHEN, *Solid-State Electron.* **10** (1967) 33.
8. D. SHAW, editor, "Atomic diffusion in semiconductors" (Plenum Press, London and New York, 1973), Chapter 5.
9. R. D. SHANNON and C. T. PREWITT, *Acta Cryst.* **B25** (1969) 925.
10. I. WALLER, *Ann. Phys.* **79** (1926) 261.
11. B. W. BATTERMAN and H. COLE, *Rev. Mod. Phys.* **36** (1964) 681.
12. A. W. WARNER, M. ONOE, and G. A. COQUIN, *J. Acoust. Soc. Am.* **42** (1967) 1223.
13. J. F. NYE, "Physical properties of crystals" (Oxford University Press, 1957), p. 249.
14. J. E. MIDWINTER, *J. Appl. Phys.* **39** (1968) 3033.
15. R. J. O'BRIEN, G. J. ROSASCO, and A. WEBER, *J. Opt. Soc. Am.* **60** (1970) 716.
16. C. KITTEL, "Introduction to solid state physics", 2nd edition, (Wiley Inc., New York, 1956), p. 165.
17. H. IWASAKI, T. YAMADA, N. NIIZEKI, and H. TOYODA, *Rev. ECL* **16** (1968) 385.
18. A. SAVAGE, *J. Appl. Phys.* **37** (1966) 3071.

Received 27 April and accepted 20 May 1977.